

Harnessing Environmental Memory with Reinforcement Learning in Open Quantum Systems

Safae Gaidi ¹, Abdallah Slaoui ^{1,2}, Mohammed EL Falaki ¹ and Amine Jaouadi ^{3,*}

¹*LPHE-MS, Faculty of Sciences, Mohammed V University in Rabat, Rabat, Morocco*

²*CPM, Faculty of Sciences, Mohammed V University in Rabat, Rabat, Morocco.*

³*LyRIDS, ECE-Paris School of Engineering, 10 rue Sextius Michel, 75015 Paris - France*

(Dated: January 6, 2026)

Non-Markovian memory effects in open quantum systems provide valuable resources for preserving coherence and enhancing controllability; however, exploiting them requires strategies adapted to history-dependent dynamics. We introduce a reinforcement-learning framework that autonomously learns to amplify information backflow in a driven two-level system coupled to a structured reservoir. Using a reward based on the positive time derivative of the trace distance associated with the Breuer–Laine–Piilo measure, we train PPO and SAC agents and benchmark their performance against gradient-based optimal control theory (OCT). While OCT enhances a single dominant backflow peak, RL policies broaden this revival and activate additional contributions in later memory windows, producing sustained positive trace-distance growth over a longer duration. Consequently, the integrated non-Markovianity achieved by RL substantially exceeds that obtained with OCT. These results demonstrate how long-horizon, model-free learning naturally uncovers distributed-backflow strategies and highlight the potential of reinforcement learning for engineering memory effects in open quantum systems.

I. INTRODUCTION

Open quantum systems inevitably interact with surrounding environments, leading to decoherence, energy relaxation, and loss of distinguishability between quantum states [1, 2]. In many physical platforms from solid-state spins and superconducting qubits to nanophotonic structures and molecular systems the environment is structured or strongly coupled, and its correlations persist on timescales comparable to the intrinsic system dynamics. In such regimes, the reduced dynamics cannot be described by a simple Markovian semigroup and instead exhibits memory effects, revivals of coherence, and information backflow, i.e., genuinely non-Markovian behavior [3–7].

Over the past decade, non-Markovianity has been recognized as a useful resource rather than merely a nuisance. It can enhance quantum channel capacities and improve the performance of information-processing tasks [8–10], enable noise reduction beyond the reach of standard dynamical decoupling [11], and offer advantages in quantum metrology and sensing when suitably controlled [12–14]. Recent work has also highlighted the relevance of non-Markovianity for quantum machine learning, where environmental memory can boost the effective memory of quantum neural-network architectures [15]. These advances support a resource-theoretic view in which non-Markovian dynamics, viewed as multi-time quantum processes, can be harnessed and transformed by appropriate control operations [16, 17]

From a theoretical standpoint, controlling non-Markovian dynamics is challenging. Memory kernels,

time-nonlocal master equations, or time-dependent decay rates such as $\gamma(t)$ in time-local formulations lead to control landscapes that are highly non-convex and history dependent [18, 19]. Standard optimal control theory (OCT) methods, which have been remarkably successful in Markovian and closed-system settings [20–22], rely on the computation of gradients of a final-time cost functional with respect to control fields. In the presence of memory, these gradients become sensitive to numerical approximations and to the full past trajectory, which can lead to unstable optimization and trapping in local optima [23, 24]. This difficulty is amplified when the figure of merit is itself non-linear and temporally non-local, as is the case for most non-Markovianity measures.

In parallel, there has been rapid progress in using machine learning to characterize and exploit non-Markovian dynamics. Data-driven schemes have been proposed to reconstruct memory kernels and effective environments directly from experimental trajectories [25, 26], and to analyze complex memory effects in many-body systems [27, 28]. These approaches highlight that non-Markovianity can be accessed operationally through repeated interaction and statistical learning, without the need for an exact microscopic model.

Reinforcement learning (RL) naturally fits within this paradigm. In RL, an agent learns a control policy by interacting with the system and maximizing a scalar reward signal [29, 30]. RL has been successfully applied to quantum state preparation, gate design, and feedback control in both simulations and experiments [31–33]. In particular, RL can be implemented in a model-free fashion directly on hardware, allowing control strategies to adapt to the specific, possibly non-Markovian noise of the device [34, 35]. Recent work has begun to combine RL with physics-informed constraints and model-based elements to improve sample efficiency and robustness in

* ajaouadi@ece.fr

open quantum systems [36, 37].

Very recently, RL has also been explored explicitly in non-Markovian settings. Hybrid schemes integrating model learning and RL have been proposed for spin-boson models with memory [38], RL has been shown to provide an efficient alternative to conventional OCT in non-Markovian molecular control problems [22]. At the same time, independent developments in non-Markovian quantum control and reservoir engineering [19, 39] underscore the importance of designing control protocols that are sensitive to the temporal structure of environmental memory.

In this work, we bring together these threads by investigating how modern RL methods can actively exploit environmental memory in a minimal yet representative open quantum system. We consider a driven two-level system coupled to a Lorentzian reservoir, where the time-dependent decay rate $\gamma(t)$ can become temporarily negative, signaling information backflow [40–42]. Using measure of non-Markovianity as our objective, we design a reward that directly favors episodes of positive trace-distance growth and implement both a Soft Actor-Critic(SAC) and a Proximal Policy Optimization (PPO) agent to learn continuous control fields [43–45]. We benchmark these RL policies against classical OCT with Powell and L-BFGS-B. We show that OCT produces sharp, high-amplitude revivals in the instantaneous non-Markovianity rate, whereas RL policies generate a sequence of more moderate revivals that persist over a longer fraction of the evolution time. This redistribution in time leads to a higher total integrated non-Markovianity for RL than for OCT, with PPO achieving the largest overall enhancement and SAC delivering smoother, experimentally attractive pulses. Our results contribute to the emerging view of non-Markovianity as an operational resource and illustrate how RL can serve as a flexible, model-free tool for non-Markovian quantum control.

II. THEORETICAL MODEL

We consider a driven two-level system with Hamiltonian

$$H(t) = \frac{\Delta}{2}\sigma_z + \frac{\Omega(t)}{2}\sigma_x, \quad (1)$$

where Δ is the detuning and $\Omega(t)$ is a controllable driving field. The system interacts with a structured bosonic reservoir, resulting in a time-local master equation [1]:

$$\dot{\rho}(t) = -i[H(t), \rho(t)] + \gamma(t)(\sigma_- \rho \sigma_+ - \frac{1}{2}\{\sigma_+ \sigma_-, \rho\}). \quad (2)$$

For a Lorentzian spectral density, the decay rate is [5, 6]:

$$\gamma(t) = \Re \left[\frac{2\Gamma\lambda \sinh(dt/2)}{d \cosh(dt/2) + \lambda \sinh(dt/2)} \right], \quad (3)$$

where $d = \sqrt{\lambda^2 - 2\Gamma\lambda}$. When $\Gamma > \lambda/2$, the decay rate becomes negative in certain intervals—a signature of information backflow and non-Markovianity.

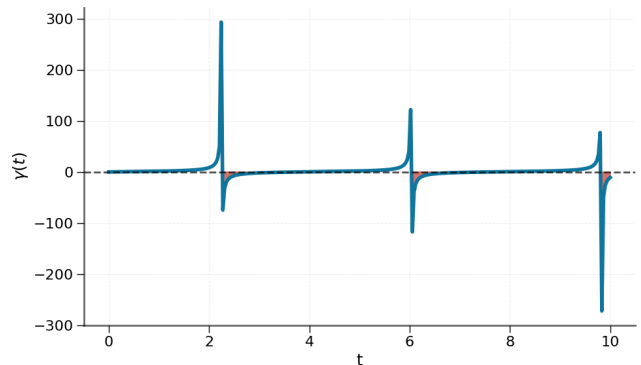


FIG. 1. Time-dependent decay rate $\gamma(t)$ for a Lorentzian spectral density in the strong-coupling regime $\Gamma > \lambda/2$. The regions where $\gamma(t) < 0$ (shaded in red) correspond to non-Markovian intervals where information flows back into the system.

The quantity $\gamma(t)$ plays a central role in characterizing memory effects. In the weak-coupling regime $\Gamma < \lambda/2$, $\gamma(t)$ remains strictly positive and the dynamics is CP-divisible, corresponding to a Markovian amplitude-damping process. In contrast, for $\Gamma > \lambda/2$, the decay rate exhibits pronounced oscillations with intervals of negativity. These $\gamma(t) < 0$ windows signal genuine information backflow from the environment into the system and thus constitute the non-Markovian regime [3, 4, 6]. A representative example is shown in Fig. 1, where negative segments of $\gamma(t)$ mark the times at which memory revivals can occur.

III. NON-MARKOVIANITY MEASURE

We quantify information backflow using the BLP measure [3], based on the trace distance:

$$D(t) = \frac{1}{2} \|\rho_1(t) - \rho_2(t)\|. \quad (4)$$

An increase in distinguishability,

$$\dot{D}(t) > 0, \quad (5)$$

indicates information flowing from the environment back into the system.

We define the instantaneous non-Markovianity rate

$$\mathcal{N}_{\text{loc}}(t) = \max[0, \dot{D}(t)], \quad (6)$$

and the total non-Markovianity over the interval $[0, T]$:

$$\mathcal{N}_{\text{Tot}} = \int_0^T \mathcal{N}_{\text{loc}}(t) dt. \quad (7)$$

Following the standard result for amplitude-damping channels, we choose optimal initial states $\rho_1(0) = |1\rangle\langle 1|$ and $\rho_2(0) = |0\rangle\langle 0|$.

IV. OPTIMAL CONTROL THEORY

We now evaluate whether classical optimal control theory can enhance non-Markovianity by shaping the driving field $\Omega(t)$. The control pulse is parameterized as piecewise constant with N_c time bins and bounded amplitude. We use two established OCT algorithms: (i) Powell’s derivative-free method, and (ii) L-BFGS-B, a limited-memory quasi-Newton algorithm with bound constraints. These algorithms are widely used in quantum control [20].

A. OCT convergence: total non-Markovianity

To evaluate the performance of optimal control theory (OCT), we directly maximize the total non-Markovianity \mathcal{N}_{Tot} by optimizing the set of control pulse amplitudes $\{\Omega_j\}$. Figure 2 depicts the evolution of the total non-Markovianity as a function of the iteration number for the Powell and L-BFGS-B methods, highlighting their distinct convergence behaviors.

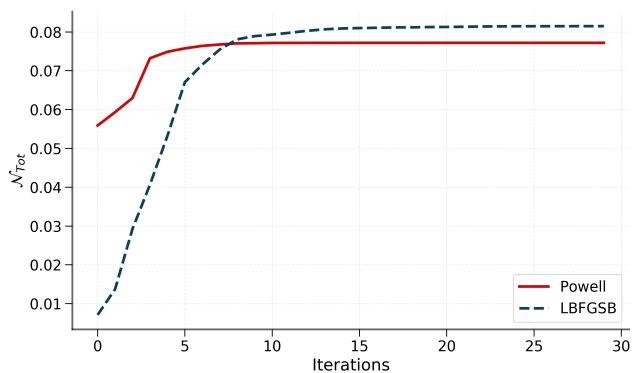


FIG. 2. Convergence history of the total non-Markovianity \mathcal{N}_{Tot} for Powell (red) and L-BFGS-B (blue). Both algorithms improve \mathcal{N}_{Tot} relative to the uncontrolled case, but rapidly plateau at different local optima, indicating the presence of a strongly non-convex control landscape shaped by memory effects.

Although both methods achieve moderate enhancement, their convergence is slow and highly sensitive to the initial guess. This behavior is consistent with observations that OCT becomes fragile when the dynamics is non-Markovian or effectively non-Markovian due to non-linear, history-dependent control objectives [20, 23].

B. OCT effect on instantaneous non-Markovianity

To visualize how OCT modifies the structure of information backflow, we inspect the instantaneous rate $\mathcal{N}_{\text{loc}}(t)$. Figure 3 compares $\mathcal{N}_{\text{loc}}(t)$ for the uncontrolled case and for the optimized pulses.

OCT enhances the revivals modestly, but never achieves their full amplification. This reflects two challenges:

1. *Temporal sensitivity* – small changes in $\Omega(t)$ shift the system’s phase relative to the backflow windows, causing irregular gradients.

2. *Landscape fragmentation* – memory-induced control landscapes contain many isolated local maxima that gradient-based methods cannot escape [23].

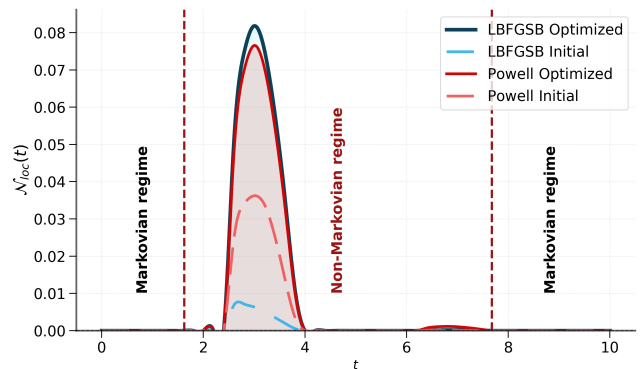


FIG. 3. Instantaneous non-Markovianity $\mathcal{N}_{\text{loc}}(t)$ for the uncontrolled dynamics and after OCT optimization with Powell (red) and L-BFGS-B (blue), illustrating modified backflow features under control.

C. Optimized OCT pulses

The optimized pulses are shown in Fig. 4. Although both algorithms start from the same amplitude bounds and pulse discretization, they converge to markedly different solutions.

These large variations between local optima even for identical optimization settings highlight the difficulty of coordinating the control field with the environmental memory structure. This fundamental limitation of OCT in memory-bearing systems has been noted in studies comparing OCT and machine-learning-based quantum control [42, 44].

V. REINFORCEMENT-LEARNING FRAMEWORK

Reinforcement learning provides an alternative to OCT that bypasses the need for model gradients or adjoint backpropagation. Rather than optimizing a functional in a fixed control landscape, the agent learns directly from trajectory data generated during system evolution. At each step, it interacts with the quantum system, observes the resulting dynamics, receives rewards proportional to information backflow, and updates a policy $\pi(\Omega|s)$ that selects the control amplitude based on the observed state.

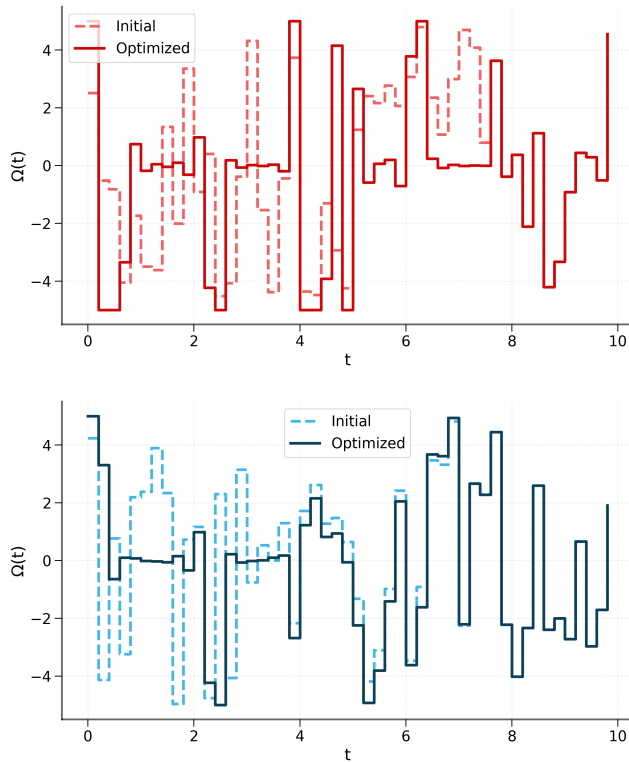


FIG. 4. Optimized control pulses $\Omega(t)$ obtained with Powell (top) and LFBGSB (bottom). The two methods converge to distinct local optima, consistent with a fragmented control landscape in the presence of non-Markovian effects.

This data-driven approach is naturally suited to non-Markovian environments, in which temporal correlations and memory revivals create rugged, highly non-convex landscapes that gradient-based methods often struggle to exploit consistently.

A. RL environment formulation

Before defining the observation and action spaces, we emphasize that the control field used here is *stepwise constant in time*. During each interval $[t_k, t_{k+1})$ of duration Δt , the driving amplitude Ω_k is held fixed and updated only at discrete decision steps. The agent nonetheless operates in a *continuous action space* ($a_k \in \mathbb{R}$), which makes the task a continuous-action RL problem while retaining the standard piecewise-constant parametrization used in quantum control.

The observation vector at time t_k is defined as

$$s_k = [t_k/T, D_k, \dot{D}_{k-1}, \gamma_k, \Omega_k], \quad (8)$$

which provides the agent with: (i) the normalized time coordinate within the episode, (ii) the distinguishability D_k between trajectories, (iii) the previous slope \dot{D}_{k-1} as an indicator of imminent backflow, (iv) the instantaneous decay rate γ_k , and (v) the current control amplitude.

The action is a continuous increment to the driving field:

$$\Omega_{k+1} = \text{clip}(\Omega_k + a_k, \Omega_{\min}, \Omega_{\max}), \quad (9)$$

from which a piecewise-constant control profile over the full episode is constructed.

The reward function directly encodes the BLP information backflow:

$$r_k = \max(0, \dot{D}_k) \approx \max\left(0, \frac{D_{k+1} - D_k}{\Delta t}\right), \quad (10)$$

encouraging the agent to detect, anticipate, and exploit intervals of positive $\dot{D}(t)$ without requiring any explicit knowledge of the analytic master equation.

B. RL algorithms: SAC and PPO

To learn optimal control strategies, we employ two complementary continuous-action RL algorithms: Soft Actor-Critic (SAC) and Proximal Policy Optimization (PPO).

SAC [41] is an off-policy actor-critic method that has shown excellent performance in quantum control tasks [43, 46]. It maximizes a stochastic objective with an entropy regularizer,

$$J(\pi) = \mathbb{E}_{(s,a) \sim \pi} [Q(s,a) - \tau \log \pi(a|s)], \quad (11)$$

promoting exploratory yet purpose-driven behavior. Three features make SAC particularly powerful in non-Markovian settings:

1. *Maximum-entropy exploration* helps discover the coordinated pulse patterns required to exploit intervals where $\gamma(t)$ becomes negative.
2. *Off-policy learning* enables extensive reuse of rare, highly informative trajectories exhibiting strong memory revivals.
3. *Twin Q-networks* mitigate value overestimation in the rugged, non-convex landscape generated by non-Markovian dynamics.

To provide a robust and interpretable baseline, we also train a PPO agent. PPO is an on-policy actor-critic method whose updates are governed by the clipped surrogate objective

$$\mathcal{L}^{\text{CLIP}} = \mathbb{E} \left[\min \left(r_k(\theta) \hat{A}_k, \text{clip}(r_k(\theta), 1 - \varepsilon, 1 + \varepsilon) \hat{A}_k \right) \right]. \quad (12)$$

Here $r_k(\theta) = \pi_\theta(a_k|s_k)/\pi_{\theta_{\text{old}}}(a_k|s_k)$ is the probability ratio comparing the new policy to the policy that generated the rollout, \hat{A}_k is the advantage estimate indicating whether the action was better or worse than expected, and ε is a clipping parameter that limits how far the policy is allowed to move in a single update. The clipping

term prevents excessively large policy shifts, promoting stable and smooth control updates. PPO additionally employs generalized advantage estimation (GAE) to obtain low-variance advantage signals, which further encourages temporally coherent adjustments to the pulse amplitude.

Although PPO is generally less sample-efficient than SAC and explores more conservatively, it is well known for reliable convergence in continuous-control tasks. In our simulations, PPO achieves a higher total non-Markovianity N_{Tot} than SAC, suggesting that its incremental update mechanism and inherent regularization toward smooth policies are well suited to the structured temporal organization of memory revivals. Contrasting PPO and SAC therefore reveals how on-policy versus off-policy learning mechanisms exploit different aspects of the temporal complexity in memory-rich quantum environments.

C. RL workflow

A schematic overview of the RL loop is shown in Fig. 5. Both SAC and PPO interact with the environment through the following sequence:

1. Initialize $\rho_1(0)$, $\rho_2(0)$, and a random initial amplitude Ω_0 .
2. Apply the action a_k and propagate the master equation for one step Δt .
3. Compute D_k , \dot{D}_k , and the reward r_k .
4. Store the transition (s_k, a_k, r_k, s_{k+1}) : SAC uses a replay buffer, while PPO uses on-policy rollouts.
5. Update the actor and critics using gradient descent according to the chosen RL algorithm.

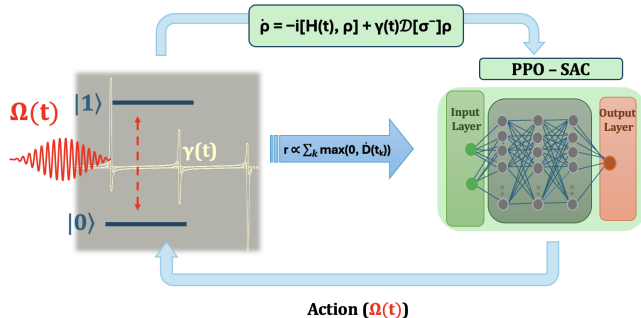


FIG. 5. Reinforcement-learning control loop for maximizing non-Markovianity. The agent observes $(D, \dot{D}, \gamma, \Omega)$, selects actions, and receives rewards based on information backflow.

VI. RESULTS AND DISCUSSION

A. OCT versus RL: peaks versus area

Figure 3 summarize the behavior of the Powell and L-BFGS-B OCT algorithms. OCT clearly increases both the height and the width of the main local non-Markovianity (solid line) compared with the uncontrolled case (dashed line). However, this enhancement remains concentrated in a relatively narrow time window around the dominant backflow episode. The instantaneous rate $\mathcal{N}_{\text{loc}}(t)$ under OCT is slightly larger than in our RL runs at its maximum, which is visible when comparing the OCT curves in Figure 3 with the RL-controlled curves discussed below in Figure 6.

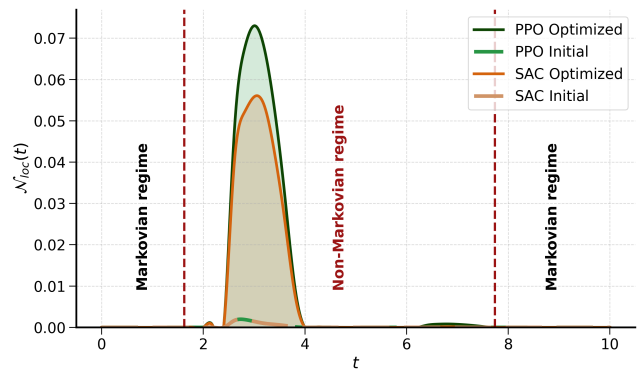


FIG. 6. Instantaneous non-Markovianity \mathcal{N}_{loc} for different control methods: no control, Powell, L-BFGS-B, PPO, and SAC. Both RL agents clearly outperform the OCT baselines in terms of integrated non-Markovianity, with PPO yielding the largest \mathcal{N}_{loc} among all tested methods.

At first sight, this might suggest that OCT should also achieve the largest total non-Markovianity \mathcal{N}_{Tot} , since it produces the largest local peaks. The surprising outcome of our study is that this intuition is wrong: the RL agents, and in particular PPO, obtain a larger integrated non-Markovianity than both Powell and L-BFGS-B, even though their $\mathcal{N}_{\text{loc}}(t)$ curves are less sharply peaked at any given time. In other words, OCT focuses the information backflow into one or two strong revivals, while RL learns to spread backflow over many milder revivals, increasing the area under $\mathcal{N}_{\text{loc}}(t)$.

This distinction is central to interpreting our results: OCT excels at producing high instantaneous backflow in a short interval. RL instead restructures the dynamics to support moderate backflow sustained over a longer period, leading to a larger time integral \mathcal{N}_{Tot} . This many-small-waves vs. one-big-wave trade-off is precisely what one expects from an agent whose reward is the time-sum of local BLP increments, rather than their maximum.

B. Global performance comparison

The global comparison is shown in Fig. 7, where we track the evolution of the total non-Markovianity \mathcal{N}_{Tot} during training for PPO and SAC. Both agents rapidly escape the low-performance regime associated with random initial pulses: within the first few hundred iterations, \mathcal{N}_{Tot} already exceeds 0.2 for both methods.

After this shared initial rise, their learning dynamics diverge. PPO exhibits a staircase-like progression marked by abrupt policy improvements, reaching its final plateau $\mathcal{N}_{\text{Tot}} \approx 0.37$ after roughly 10^3 – 1.5×10^3 iterations. SAC stabilizes early around $\mathcal{N}_{\text{Tot}} \approx 0.26$, then improves gradually through many small increments, eventually saturating near $\mathcal{N}_{\text{Tot}} \approx 0.29$. Although lower than PPO, this value still substantially exceeds those obtained with Powell and L-BFGS-B OCT.

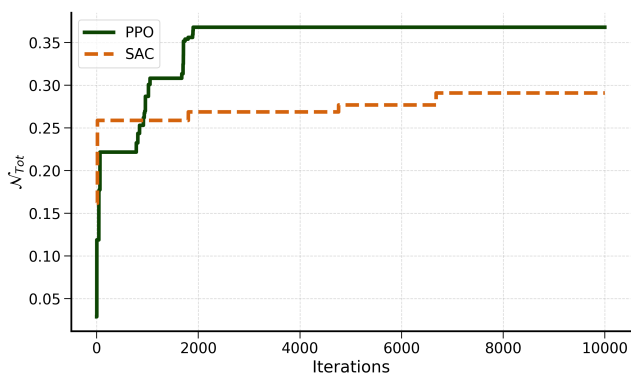


FIG. 7. Convergence history of the total non-Markovianity \mathcal{N}_{Tot} for PPO (green) and SAC (orange). Both agents rapidly improve their performance, with PPO converging faster and reaching the highest final value.

The resulting hierarchy is:

1. PPO attains the largest total non-Markovianity \mathcal{N}_{Tot} .
2. SAC reaches a slightly smaller but still strongly enhanced value.
3. OCT improves upon the uncontrolled dynamics but remains far below the RL policies in total \mathcal{N}_{Tot} .

At first sight this appears paradoxical: as shown in Fig. 3, OCT often produces slightly higher peaks in the instantaneous non-Markovianity $\mathcal{N}_{\text{loc}}(t)$ than the RL policies. The resolution lies in the shape of the curves and the definition of the BLP measure (Eq. 7). What matters is not the height of the largest peak but the total *area* under $\mathcal{N}_{\text{loc}}(t)$.

OCT, constrained by its gradient-based optimization and a landscape fragmented by memory effects, concentrates its improvements into the dominant backflow window: it sharpens and slightly broadens a single peak

while leaving the rest of the time evolution largely unaffected. The resulting profile resembles a tall, narrow “mountain” that contributes only modest area.

RL behaves fundamentally differently. Because PPO and SAC receive positive reward whenever $\dot{D}(t) > 0$, they are explicitly incentivized to sustain information backflow for as long as possible, even if each individual revival has moderate height. As shown in Fig. ??, RL broadens the main revival and—crucially—activates additional secondary revivals at later times. These contributions are individually small but collectively dominate the integral. Over many iterations the agents discover a distributed-backflow strategy that maximizes cumulative return rather than instantaneous gain.

Physically, OCT engineers a single burst of information return, whereas RL learns a temporally extended “breathing” pattern: several moderate backflow episodes of coordinated timing. Since the BLP measure rewards *duration* as well as *intensity*, this distributed strategy naturally yields a much larger \mathcal{N}_{Tot} , explaining why PPO and SAC robustly outperform OCT.

C. RL pulse shaping

To understand why PPO ultimately achieves a larger integrated non-Markovianity than SAC, we compare in Fig. 8 the optimized control pulses generated by the two agents. Although both start from similar random initial pulses, their learned solutions exhibit clear and systematic differences once training converges.

The SAC-optimized pulse (top panel) displays pronounced small-scale fluctuations and frequent abrupt jumps between amplitude values. This irregular, high-variance structure reflects the entropy-regularized objective of SAC: the policy intentionally retains some stochasticity throughout training, promoting broader exploration of the fragmented landscape but resulting in less temporally coherent pulse profiles.

By contrast, the PPO pulse (bottom panel) is noticeably smoother and more structured. Its amplitude evolves through longer and more coherent segments, with fewer rapid switches between successive time steps. This behavior follows from PPO’s clipped-surrogate update rule, which limits large policy deviations and guides the controller toward a more deterministic and stable modulation pattern once a beneficial strategy has been identified.

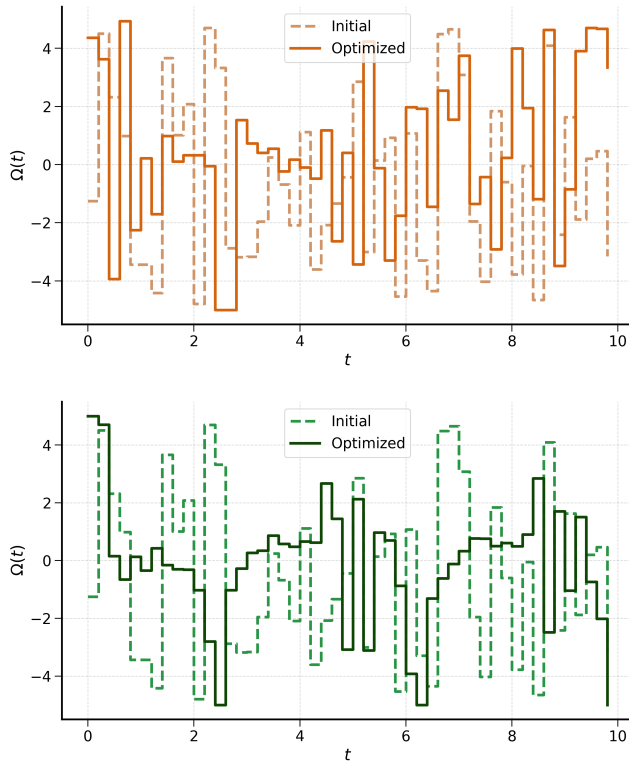


FIG. 8. Optimized control pulses obtained with SAC (top) and PPO (bottom), compared to their respective initial random pulses (dashed).

These qualitative differences translate directly into how each agent exploits the non-Markovian structure of the dynamics. As shown in Fig. 1, the system features three distinct memory-revival windows where $\gamma(t)$ becomes negative. PPO responds to these intervals with well-organized, phase-aligned amplitude patterns, enabling it to maintain $\dot{D}(t) > 0$ over longer portions of each window and thereby accumulate a larger total backflow. SAC reacts to the same regions, but its higher-variance pulse modulations produce a less consistent temporal alignment, intermittently enhancing and interrupting backflow.

From a practical standpoint, this trade-off is meaningful. PPO achieves the highest total non-Markovianity by converging to a strong and highly structured control field. SAC, while yielding a slightly lower \mathcal{N}_{Tot} , produces pulses that are less smooth but may be more flexible or easier to implement on hardware with amplitude or bandwidth constraints. Together, these differences illustrate how the algorithmic principles of PPO and SAC manifest directly in the learned control landscapes.

D. Comparative Roles and Trade-offs of PPO, SAC, and OCT

Drawing on both the learning curves and the optimized pulse structures, we can now clarify the distinct roles, strengths, and limitations of OCT, PPO, and SAC in controlling non-Markovian dynamics.

OCT enhances the dominant backflow window but is unable to redistribute information return across the full evolution. Its gradient-based updates reinforce the strongest local feature of the landscape, leading to a tall, narrow peak in $\mathcal{N}_{\text{loc}}(t)$ while leaving later revival regions essentially unaltered. Because the functional gradient carries little information outside this window, OCT saturates quickly and fails to accumulate significant integrated non-Markovianity. Memory-induced landscape fragmentation further restricts its ability to explore alternative temporal structures.

Reinforcement learning uncovers a qualitatively different strategy. Rewarded whenever $\dot{D}(t) > 0$, PPO and SAC learn to maintain positive distinguishability growth over extended portions of the evolution. Instead of concentrating all effort on one strong revival, RL broadens the main peak and activates smaller additional contributions in the later non-Markovian windows. Individually these contributions are modest, but their combined area yields a much larger total non-Markovianity \mathcal{N}_{Tot} . This distributed use of memory is precisely what the BLP integral rewards, and it allows RL to exploit temporal structure that OCT leaves unused.

Within the RL family, PPO and SAC differ in ways that reflect their algorithmic designs. PPO attains the highest \mathcal{N}_{Tot} of all methods. Its clipped on-policy updates discourage large policy shifts and promote smooth, temporally coherent control pulses that remain well aligned with multiple backflow windows. This results in sustained intervals with $\dot{D}(t) > 0$ without resorting to extreme control amplitudes.

SAC, while achieving slightly lower \mathcal{N}_{Tot} , still significantly outperforms OCT. Its entropy-regularized objective preserves controlled stochasticity, enabling broader exploration of the fragmented landscape and robust convergence. The resulting pulses exhibit more small-scale fluctuations: these can intermittently enhance backflow but may also interrupt it, leading to somewhat shorter effective durations of positive $\dot{D}(t)$. Even so, SAC achieves strong overall performance and demonstrates the utility of entropy-regularized RL for memory-rich quantum control.

In summary, OCT concentrates its effort into amplifying a single strong revival, whereas RL—especially PPO—coordinates backflow across the entire trajectory. This global, time-aware strategy enables RL to achieve substantially larger integrated non-Markovianity and to outperform OCT in both magnitude and robustness.

VII. CONCLUSION

We have developed a reinforcement-learning framework for enhancing non-Markovianity in a driven open quantum system by maximizing the BLP measure through direct trajectory-based feedback. Unlike gradient-based optimal control theory, which is limited by memory-induced landscape fragmentation and tends to amplify only the strongest revival of information backflow, reinforcement learning uncovers control strategies that exploit the full temporal structure of environmental memory.

Our numerical results establish a clear hierarchy among the methods. Both PPO and SAC achieve substantially larger total integrated non-Markovianity than Powell and L-BFGS-B OCT, even though OCT can create a slightly higher peak in $\mathcal{N}_{\text{loc}}(t)$. PPO attains the largest overall \mathcal{N}_{Tot} and converges to smooth, temporally coherent pulse sequences that synchronize effectively with multiple memory-revival windows. SAC reaches a slightly lower \mathcal{N}_{Tot} but consistently surpasses OCT, benefiting from entropy regularization and off-policy learning to maintain robust exploration and stable convergence. Its optimized pulses exhibit more small-scale variability, reflecting the stochasticity deliberately preserved in SAC and potentially offering increased robustness to modeling imperfections.

These findings highlight a qualitative advantage of reinforcement learning: rather than concentrating control resources into a single sharp backflow episode, RL learns to sustain moderate information return across several intervals of the dynamics. This distributed, time-aware coordination is exactly what the BLP integral rewards, and it explains why model-free RL controllers can consistently outperform gradient-based OCT even when local peak behavior appears comparable.

The ability of RL agents to exploit memory effects directly from observational data, without requiring analytic gradients or detailed environmental modeling, makes them promising candidates for experimental deployment in platforms where non-Markovianity is in-

trinsic or can be engineered. Future directions include extending the approach to multi-qubit architectures, feedback-enhanced bath engineering, and the integration of RL with real-time estimation protocols to actively shape memory for quantum technological applications.

ACKNOWLEDGMENTS

S.G. acknowledges the financial support of the National Center for Scientific and Technical Research (CNRST) through the ‘‘PhD-Associate Scholarship-PASS’’ program.

Appendix A: Computational Models and Integration Schemes

We summarize here the different OCT and RL routines used in this work. All algorithms operate on the vector of control amplitudes $\mathbf{\Omega} = (\Omega_1, \dots, \Omega_{N_c})$ defining the piecewise constant pulse $\Omega(t)$, and attempt to maximize the total non-Markovianity $\mathcal{N}_{\text{Tot}}(\mathbf{\Omega})$ obtained from a full master-equation propagation.

For completeness, we summarize the hyper-parameters values used in PPO and SAC algorithms in I.

TABLE I. Key hyperparameters of the reinforcement learning algorithms used for non-Markovian control.

Parameter	SAC	PPO
Hidden layers	[256, 256]	[64, 64]
Learning rate	3×10^{-4}	6×10^{-4}
Batch size	256	64
Buffer size	300,000	–
Total training steps	5×10^5	5×10^5
Action range	[-5,5]	[-5,5]
Seed	42	42

-
- [1] H.-P. Breuer and F. Petruccione, *The Theory of Open Quantum Systems* (Oxford University Press, 2002).
- [2] Á. Rivas and S. F. Huelga, *Open Quantum Systems: An Introduction* (Springer, 2012).
- [3] H.-P. Breuer, E.-M. Laine, and J. Piilo, ‘‘Measure for the degree of non-Markovian behavior of quantum processes in open systems,’’ *Phys. Rev. Lett.* **103**, 210401 (2009).
- [4] Á. Rivas, S. F. Huelga, and M. B. Plenio, ‘‘Quantum non-Markovianity: Characterization, quantification and detection,’’ *Rep. Prog. Phys.* **77**, 094001 (2014).
- [5] S. Gaidi, A. Slaoui, M. E. Falaki, and R. A. Laamara, ‘‘Impact of non-Markovianity on quantum precision and synchronization in open quantum systems,’’ *Physica A* **581**, 131129 (2025).
- [6] I. de Vega and D. Alonso, ‘‘Dynamics of non-Markovian open quantum systems,’’ *Rev. Mod. Phys.* **89**, 015001 (2017).
- [7] S. Shrikant and F. Petruccione, ‘‘Quantum non-Markovianity: Characterization, quantification, and applications,’’ *Advances in Physics: X* **8**, 2161277 (2023).
- [8] D. Chruściński and S. Maniscalco, ‘‘Degree of non-Markovianity of quantum evolution,’’ *Phys. Rev. Lett.* **112**, 120404 (2014).
- [9] B. Bylicka, D. Chruściński, and S. Maniscalco, ‘‘Non-Markovianity and reservoir memory of quantum channels,’’ *Scientific Reports* **4**, 5720 (2014).
- [10] Y. Dakir, et al., ‘‘Quantifying non-Markovianity via local quantum Fisher information,’’ *arXiv preprint*

- arXiv:2409.10163 (2024).
- [11] G. D. Berk, Y. C. Chan, M. Gessner, W. K. Tham, and A. Acín, “Non-Markovianity as a resource for quantum noise suppression,” *PRX Quantum* **4**, 020318 (2023).
- [12] N.-E. Abouelkhir, S. Gaidi, A. Slaoui, and R. A. Laamara, “A simple analytical expression of quantum Fisher and Skew information and their dynamics under decoherence channels,” *Physica A* **612**, 128479 (2023).
- [13] P. Yang, et al., “Non-Markovianity-enhanced quantum metrology via optimal probing strategies,” *Physical Review A* **109**, 012202 (2024).
- [14] N.-E. Abouelkhir, A. Slaoui, and R. A. Laamara, “Quantum phase sensitivity with generalized coherent states based on deformed $su(1,1)$ and Heisenberg algebras,” *Ann. Phys.* **483**, 170276 (2025).
- [15] M. Sannia, M. Cattaneo, and M. Ciccarello, “Environmental memory boosts the expressivity of quantum recurrent neural networks,” *PRX Quantum* **6**, 010301 (2025).
- [16] A. Jaouadi, et al., “Exceptional points for logic operations at the molecular level,” *Fortschritte der Physik* **61**, 162–177 (2013).
- [17] G. D. Berk, L. D. Salvia, W. K. Tham, and A. Acín, “Resource theory of non-Markovianity for multi-time quantum processes,” *Quantum* **5**, 528 (2021).
- [18] V. E. Tarasov and M. Li, “Fractional dynamics of open quantum systems and non-Markovian master equations,” *Physics Reports* **923**, 1–65 (2021).
- [19] W. Wu, X. Jin, Z. Zheng, and R. Wu, “Non-Markovian trajectory tracking and optimal control of open quantum systems,” *Physical Review A* **105**, 022614 (2022).
- [20] M. H. Goerz, D. M. Reich, and C. P. Koch, “Optimal control theory for a unitary operation under dissipative evolution,” *New J. Phys.* **16**, 055012 (2014).
- [21] S. J. Glaser, U. Boscain, T. Calarco, C. P. Koch, W. Köckenberger, R. Kosloff, I. Kuprov, B. Luy, S. Schirmer, T. Schulte-Herbrüggen, D. Sugny, and F. Wilhelm, “Training Schrödinger’s cat: Quantum optimal control: Strategic report on current status, visions and goals for research in Europe,” *Eur. Phys. J. D* **69**, 279 (2015).
- [22] A. Jaouadi, E. Mangaud, and M. Desouter-Lecomte, “Re-exploring control strategies in a non-Markovian open quantum system by reinforcement learning,” *Physical Review A* **109**, 013104 (2024).
- [23] C. P. Koch, M. H. Goerz, and S. J. Glaser, “Quantum optimal control in quantum technologies: Strategic report on current status, visions and goals for research in Europe,” *EPJ Quantum Technology* **9**, 19 (2022).
- [24] C. P. Koch, M. H. Goerz, and S. J. Glaser, “Quantum optimal control in quantum technologies: Strategic report on current status, visions and goals for research in Europe,” *EPJ Quantum Technology* **9**, 19 (2022).
- [25] I. A. Luchnikov, S. V. Vintskevich, D. V. Fedorov, and S. N. Filippov, “Machine learning non-Markovian quantum dynamics,” *Physical Review Letters* **124**, 140502 (2020).
- [26] I. A. Luchnikov, H. Ouerdane, and S. N. Filippov, “Probabilistic approach to non-Markovian quantum dynamics: A reinforcement learning perspective,” *Physical Review A* **105**, 012215 (2022).
- [27] X. Han, C.-Y. Hsieh, H. Zhao, W. Li, and A. Eisfeld, “Information backflow and memory effects in open interacting quantum systems,” *Physical Review A* **106**, 012218 (2022).
- [28] N. Triviño, A. M. Alonso, and D. Alonso, “Memory-induced topological transitions in non-Markovian two-band models,” *Physical Review B* **109**, 075129 (2024).
- [29] R. S. Sutton and A. G. Barto, *Reinforcement Learning: An Introduction*, 2nd ed. (MIT Press, 2018).
- [30] D. Silver, *Lecture Notes on Reinforcement Learning* (DeepMind, 2021).
- [31] M. Bukov, A. G. Day, D. Sels, P. Weinberg, A. Polkovnikov, and P. Mehta, “Reinforcement learning in different phases of quantum control,” *Phys. Rev. X* **8**, 031086 (2018).
- [32] T. Comparin, F. Mezzacapo, and T. Roscilde, “Multipartite Entangled States in Dipolar Quantum Simulators,” *Phys. Rev. Lett.* **129** (2022) 150503.
- [33] F. Khalid, M. Skolik, G. Carleo, and H. J. Briegel, “Sample-efficient model-based reinforcement learning for quantum control,” *Machine Learning: Science and Technology* **4**, 015018 (2023).
- [34] V. V. Sivak, et al., “Model-free quantum control with deep reinforcement learning for superconducting qubits,” *Nature Physics* **17**, 1117–1121 (2021).
- [35] Y. Baum, G. Calajo, and O. E. Diaz, “Experimental deep reinforcement learning of robust quantum gates with trapped ions,” *Nature Machine Intelligence* **3**, 838–845 (2021).
- [36] M. Ernst, H. Chung, and M. Sels, “Physics-informed reinforcement learning for optimal quantum control,” *npj Quantum Information* **11**, 22 (2025).
- [37] W. Li, O. Bény, and M. Medina, “Learning quantum control policies from demonstrations: A hybrid RL approach,” *Physical Review A* **111**, 012605 (2025).
- [38] N. Neema, S. Hegde, and M. Sanz, “Non-Markovian quantum control via hybrid learning of dynamical maps and optimal policies,” *Physical Review A* **110**, 022202 (2024).
- [39] M. Lacroix, N. Fischer, and M. Knap, “Spatiotemporal control from non-Markovian dissipation in engineered quantum systems,” *Physical Review Letters* **133**, 060402 (2024).
- [40] S. Gaidi, et al., “A non-Markovianity measure based on quantum speed limit,” *Physica A: Statistical Mechanics and its Applications*, 130733 (2025).
- [41] T. Haarnoja, A. Zhou, P. Abbeel, and S. Levine, “Soft actor-critic: Off-policy maximum entropy deep reinforcement learning with a stochastic actor,” In *Proceedings of the International Conference on Machine Learning*, 1861–1870 (PMLR, July 2018).
- [42] T. Fösel, P. Tighineanu, T. Weiss, and F. Marquardt, “Reinforcement learning with neural networks for quantum feedback,” *Phys. Rev. X* **8**, 031084 (2018).
- [43] M. Y. Niu, S. Boixo, V. Smelyanskiy, and H. Neven, “Universal quantum control through deep reinforcement learning,” *npj Quantum Information* **5**, 33 (2019).
- [44] S. Li, Z. Liu, Y. Chen, H. Zhang, and D. Dong, “Robust quantum control using reinforcement learning from demonstration,” *npj Quantum Information* **11**, 124 (2025).
- [45] M. H. Goerz, S. C. Carrasco, and V. S. Malinovsky, “Quantum optimal control via semi-automatic differentiation,” *Quantum* **6**, 871 (2022).
- [46] Z. An and D. L. Zhou, “Deep reinforcement learning for quantum gate control,” *Europhys. Lett.* **126**, 60002 (2019).

Algorithm 1: Powell OCT

Input: initial control vector $\boldsymbol{\Omega}^{(0)} \in [\Omega_{\min}, \Omega_{\max}]^{N_c}$, initial set of search directions $\{\mathbf{d}_1, \dots, \mathbf{d}_{N_c}\}$ (e.g. canonical basis), maximum number of outer iterations N_{iter} .

Objective: maximize $\mathcal{N}(\boldsymbol{\Omega}) = \sum_k \max(0, \dot{D}(t_k)) \Delta t$.

1. **Initialize** iteration counter $m = 0$ and evaluate $\mathcal{N}^{(0)} = \mathcal{N}(\boldsymbol{\Omega}^{(0)})$ by:

- (a) constructing the piecewise-constant pulse $\Omega(t)$ from $\boldsymbol{\Omega}^{(0)}$;
- (b) propagating the master equation over $[0, T]$;
- (c) computing $\dot{D}(t_k)$, $\mathcal{N}_{\text{loc}}(t_k)$ and $\mathcal{N}^{(0)}$.

2. **Repeat** for $m = 0, 1, 2, \dots, N_{\text{iter}} - 1$:

(a) Set $\boldsymbol{\Omega}_{\text{start}} = \boldsymbol{\Omega}^{(m)}$ and $\mathcal{N}_{\text{start}} = \mathcal{N}^{(m)}$.

(b) **Cyclic line searches:**

i. For $j = 1, \dots, N_c$:

A. Define a 1D search along direction \mathbf{d}_j :

$$\boldsymbol{\Omega}(\lambda) = \boldsymbol{\Omega}^{(m)} + \lambda \mathbf{d}_j.$$

B. Perform a line search over λ (respecting the amplitude bounds) to find

$$\lambda^* = \arg \max_{\lambda} \mathcal{N}(\boldsymbol{\Omega}(\lambda)),$$

where each evaluation of \mathcal{N} requires a full master-equation propagation.

C. Update the control:

$$\boldsymbol{\Omega}^{(m)} \leftarrow \boldsymbol{\Omega}(\lambda^*), \quad \mathcal{N}^{(m)} \leftarrow \mathcal{N}(\boldsymbol{\Omega}^{(m)}).$$

(c) **Direction update:**

- Compute the net displacement $\mathbf{d}_{\text{new}} = \boldsymbol{\Omega}^{(m)} - \boldsymbol{\Omega}_{\text{start}}$.
- Optionally discard the oldest direction and append \mathbf{d}_{new} to $\{\mathbf{d}_1, \dots, \mathbf{d}_{N_c}\}$, following Powell's rule, to capture curvature information.

(d) **Stopping criterion:**

- If $\mathcal{N}^{(m)} - \mathcal{N}_{\text{start}}$ or $\|\mathbf{d}_{\text{new}}\|$ falls below a small threshold, stop.

Output: optimized control vector $\boldsymbol{\Omega}^*$ and pulse $\Omega^*(t)$ corresponding to a (possibly local) maximum of \mathcal{N} .

FIG. 9. Pseudocode for Powell's derivative-free optimal-control algorithm applied to the maximization of total non-Markovianity.

Algorithm 2: L-BFGS-B OCT

Input: initial control vector $\boldsymbol{\Omega}^{(0)} \in [\Omega_{\min}, \Omega_{\max}]^{N_c}$, step-size and convergence tolerances, finite-difference step ϵ , maximum number of iterations N_{iter} .

Objective: maximize $\mathcal{N}(\boldsymbol{\Omega})$ under bound constraints $\Omega_{\min} \leq \Omega_j \leq \Omega_{\max}$.

1. **Initialize** iteration $m = 0$ and evaluate $\mathcal{N}^{(0)} = \mathcal{N}(\boldsymbol{\Omega}^{(0)})$ via a full master-equation propagation.
2. **Repeat** for $m = 0, 1, 2, \dots, N_{\text{iter}} - 1$:

(a) **Gradient estimation (finite differences):**

- i. For $j = 1, \dots, N_c$:

- A. Construct a perturbed control vector $\boldsymbol{\Omega}_{(j)}^{(m)}$ by replacing $\Omega_j^{(m)} \rightarrow \Omega_j^{(m)} + \epsilon$ (and clipping to bounds).
- B. Evaluate the perturbed cost $\mathcal{N}_{(j)} = \mathcal{N}(\boldsymbol{\Omega}_{(j)}^{(m)})$ by a full propagation.
- C. Form the numerical gradient component

$$g_j^{(m)} = \frac{\mathcal{N}_{(j)} - \mathcal{N}^{(m)}}{\epsilon}.$$

- ii. Assemble the gradient vector $\mathbf{g}^{(m)} = (g_1^{(m)}, \dots, g_{N_c}^{(m)})$.

(b) **Quasi-Newton step (L-BFGS-B update):**

- i. Use the past history of $(\boldsymbol{\Omega}^{(m')}, \mathbf{g}^{(m')})$ for $m' < m$ to build a low-rank approximation of the inverse Hessian $H^{(m)}$ (in standard L-BFGS fashion).
- ii. Compute the search direction

$$\mathbf{p}^{(m)} = H^{(m)} \mathbf{g}^{(m)}.$$

- iii. Perform a line search along $\mathbf{p}^{(m)}$ (with bound handling) to find a step size $\eta^{(m)}$ maximizing \mathcal{N} :

$$\boldsymbol{\Omega}^{(m+1)} = \text{Proj}_{[\Omega_{\min}, \Omega_{\max}]^{N_c}} \left(\boldsymbol{\Omega}^{(m)} + \eta^{(m)} \mathbf{p}^{(m)} \right),$$

where Proj denotes component-wise clipping.

- iv. Evaluate $\mathcal{N}^{(m+1)} = \mathcal{N}(\boldsymbol{\Omega}^{(m+1)})$.

(c) **Stopping criterion:**

- If $\|\mathbf{g}^{(m)}\|$ and $|\mathcal{N}^{(m+1)} - \mathcal{N}^{(m)}|$ fall below given tolerances, terminate.

Output: optimized control vector $\boldsymbol{\Omega}^*$ and pulse $\Omega^*(t)$ returned by the L-BFGS-B quasi-Newton procedure.

FIG. 10. Pseudocode for L-BFGS-B optimal control applied to the maximization of total non-Markovianity with bound-constrained pulse amplitudes.

Algorithm 3: PPO

Input: initial policy parameters θ , value-function parameters ψ , control bounds $[\Omega_{\min}, \Omega_{\max}]$, episode length N_t , hyperparameters $(\gamma_{\text{RL}}, \lambda_{\text{GAE}}, \epsilon)$.

1. **Initialize** policy $\pi_\theta(a|s)$ and value network $V_\psi(s)$.

2. **Repeat** (for episodes $e = 1, 2, \dots$):

(a) **Reset environment:**

- Set $\rho_1(0) = |1\rangle\langle 1|$, $\rho_2(0) = |0\rangle\langle 0|$.
- Choose initial Ω_0 within bounds.
- Construct initial state $s_0 = (0, D_0, \dot{D}_{-1}, \gamma_0, \Omega_0)$.

(b) **Rollout generation:**

i. For $k = 0, \dots, N_t - 1$:

- A. Sample action $a_k \sim \pi_\theta(\cdot|s_k)$.
- B. Update control:

$$\Omega_{k+1} = \text{clip}(\Omega_k + a_k, \Omega_{\min}, \Omega_{\max}).$$

- C. Propagate ρ_1, ρ_2 from t_k to t_{k+1} under Ω_{k+1} .
- D. Compute D_{k+1} , \dot{D}_{k+1} and reward

$$r_k = \max(0, \dot{D}_{k+1}) - \alpha(\Delta\Omega_k)^2 - \beta\Omega_{k+1}^2.$$

- E. Form next state s_{k+1} .
- F. Store (s_k, a_k, r_k, s_{k+1}) in a trajectory buffer.

(c) **Advantage estimation:**

- Using the trajectory $\{(s_k, a_k, r_k)\}$ and V_ψ , compute advantages A_k with generalized advantage estimation (GAE) and returns R_k (targets for V_ψ).

(d) **Policy and value update:**

i. Define importance sampling ratio

$$r_k = \frac{\pi_\theta(a_k|s_k)}{\pi_{\theta_{\text{old}}}(a_k|s_k)}.$$

ii. Maximize the clipped surrogate

$$L(\theta) = \mathbb{E}[\min(r_k A_k, \text{clip}(r_k, 1 - \epsilon, 1 + \epsilon) A_k)]$$

using gradient ascent on θ .

iii. Minimize mean-squared error

$$L_V(\psi) = \mathbb{E}[(V_\psi(s_k) - R_k)^2]$$

using gradient descent on ψ .

(e) Set $\theta_{\text{old}} \leftarrow \theta$ and repeat.

Output: trained PPO policy $\pi_\theta(a|s)$ that maximizes total non-Markovianity \mathcal{N} .

FIG. 11. Pseudocode for PPO applied to maximizing the BLP non-Markovianity measure.

Algorithm 4: SAC

Input: policy parameters θ , Q-network parameters (ϕ_1, ϕ_2) , target-Q parameters $(\bar{\phi}_1, \bar{\phi}_2)$, entropy temperature τ , replay buffer \mathcal{D} , control bounds $[\Omega_{\min}, \Omega_{\max}]$, episode length N_t .

1. **Initialize** stochastic policy $\pi_\theta(a|s)$, Q-networks Q_{ϕ_1}, Q_{ϕ_2} , and target networks $Q_{\bar{\phi}_i} \leftarrow Q_{\phi_i}$.

2. **Repeat** (for episodes $e = 1, 2, \dots$):

(a) Reset environment as in Algorithm 11 to obtain s_0 .

(b) **Rollout and data collection:**

i. For $k = 0, \dots, N_t - 1$:

A. Sample action $a_k \sim \pi_\theta(\cdot|s_k)$.

B. Update control:

$$\Omega_{k+1} = \text{clip}(\Omega_k + a_k, \Omega_{\min}, \Omega_{\max}).$$

C. Propagate ρ_1, ρ_2 from t_k to t_{k+1} , compute D_{k+1}, \dot{D}_{k+1} and reward r_k as in Algorithm 11.

D. Form s_{k+1} and store transition (s_k, a_k, r_k, s_{k+1}) in replay buffer \mathcal{D} .

(c) **Parameter updates:**

i. For several gradient steps per episode:

A. Sample a minibatch of transitions $(s, a, r, s') \sim \mathcal{D}$.

B. Sample next actions $a' \sim \pi_\theta(\cdot|s')$.

C. Compute target value

$$y(r, s') = r + \gamma_{\text{RL}} [\min_i Q_{\bar{\phi}_i}(s', a') - \tau \log \pi_\theta(a'|s')].$$

D. Update Q-networks by minimizing

$$L_Q(\phi_i) = \mathbb{E}_{\mathcal{D}} [(Q_{\phi_i}(s, a) - y)^2]$$

for $i = 1, 2$.

E. Update the policy by minimizing

$$L_\pi(\theta) = \mathbb{E}_{s \sim \mathcal{D}, a \sim \pi_\theta} [\tau \log \pi_\theta(a|s) - \min_i Q_{\phi_i}(s, a)].$$

F. Update target networks with a soft update:

$$\bar{\phi}_i \leftarrow \tau_{\text{target}} \phi_i + (1 - \tau_{\text{target}}) \bar{\phi}_i.$$

Output: trained SAC policy $\pi_\theta(a|s)$ that maximizes total non-Markovianity \mathcal{N} via entropy-regularized learning.

FIG. 12. Pseudocode for SAC applied to maximizing the BLP non-Markovianity measure in the driven open quantum system.